Compressed Channel Estimation for Intelligent Reflecting Surface-Assisted Millimeter Wave Systems

Peilan Wang, Jun Fang, Huiping Duan, and Hongbin Li, *Fellow, IEEE*

***Abstract*—In this letter, we consider channel estimation for intelligent reflecting surface (IRS)-assisted millimeter wave (mmWave) systems, where an IRS is deployed to assist the data transmission from the base station (BS) to a user. It is shown that for the purpose of joint active and passive beamforming, the knowledge of a large-size cascade channel matrix needs to be acquired. To reduce the training overhead, the inherent sparsity in mmWave channels is exploited. By utilizing properties of Katri-Rao and Kronecker products, we find a sparse representation of the cascade channel and convert cascade channel estimation into a sparse signal recovery problem. Simulation results show that our proposed method can provide an accurate channel estimate and achieve a substantial training overhead reduction.**

***Index Terms*—Intelligent reflecting surface, millimeter wave communications, channel estimation.**

I. Introduction

INTELLIGENT reflecting surface (IRS) comprising a large number of passive reflecting elements is emerging as a promising technology for realizing a smart and programmable wireless propagation environment via software-controlled reflection [1]–[4]. With a smart controller, each element can independently reflect the incident signal with a reconfigurable amplitude and phase shift. By properly adjusting the phase shifts of the passive elements, the reflected signals can add coherently at the desired receiver to improve the signal power. Recently, IRS was introduced to establish robust mmWave connections when the line-of-sight (LOS) link is blocked by obstructions [5], [6]. To reach the full potential of IRSs, accurate channel state information (CSI) is required for joint active and passive beamforming. There are already some works on channel estimation for IRS-aided wireless systems, e.g., [7]–[11]. In [7], to facilitate channel estimation, active elements were used at the IRS. These active elements can operate in a receive mode so that they can receive incident signals to help estimate the BS-IRS channel and the IRS-user channel. IRSs with active elements, however, need wiring or battery power, which may not be feasible for many applications. For IRSs with all passive elements, least square (LS) estimation methods [8], [9] were proposed to estimate uplink cascade channels. The problem lies in that the cascade channel usually has a large size. These methods which do not exploit the sparse structure inherent in wireless channels may incur a considerable amount of training overhead. In [10], a sparse matrix factorization-based channel estimation method was developed by exploiting the low-rank structure of the BS-IRS and IRS-user channels. The proposed method requires to switch off some passive elements at each time. Implementing the ON/OFF switching, however, is costly as this requires separate amplitude control of each IRS element [11].

In this letter, we consider the problem of channel estimation for IRS-assisted mmWave systems. To reduce the training overhead, sparsity inherent in mmWave channels is exploited. By utilizing properties of the Khatri-Rao and Kronecker products, we find a sparse representation of the concatenated BS-IRS-user (cascade) channel. Channel estimation can then be cast as a sparse signal recovery problem and existing compressed-sensing methods can be employed. Simulation results show that our proposed method, with only a small amount of training overhead, can provide reliable channel estimation and help attain a decent beamforming gain.

II. System Model and Problem Formulation

We consider an IRS-assisted mmWave downlink system, where an IRS is deployed to assist the data transmission from the BS to a single-antenna user. Suppose the IRS is a planar array with M reflecting elements. The BS is equipped with N antennas. Let $\boldsymbol{G} \in \mathbb{C}^{M\times N}$ denote the channel from the BS to the IRS, and $\boldsymbol{h}_r \in \mathbb{C}^M$ denote the channel from the IRS to the user. To better illustrate our idea, we neglect the direct link from the BS to the user. Nevertheless, the extension to the scenario with direct link from the BS to the user is straightforward. Each reflecting element of the IRS can reflect the incident signal with a reconfigurable phase shift and amplitude via a smart controller [3]. Denote

$$\boldsymbol{\Theta} \triangleq \text{diag}(\beta_1 e^{j\theta_1}, \ldots, \beta_M e^{j\theta_M}) \tag{1}$$

as the phase-shift matrix of the IRS, where $\theta_m \in [0, 2\pi]$ and $\beta_m \in [0, 1]$ denote the phase shift and amplitude reflection coefficient associated with the mth passive element of the IRS,

Manuscript received April 10, 2020; accepted May 21, 2020. Date of publication May 28, 2020; date of current version June 11, 2020. This work was supported in part by the National Science Foundation of China under Grant 61829103 and Grant 61871421. The associate editor coordinating the review of this manuscript and approving it for publication was Dr. Michael Joham. *(Corresponding author: Jun Fang.)*

Peilan Wang and Jun Fang are with the National Key Laboratory of Science and Technology on Communications, University of Electronic Science and Technology of China, Chengdu 611731, China (e-mail: peilan_wangle@std.uestc.edu.cn; junfang@uestc.edu.cn).

Huiping Duan is with the School of Information and Communications Engineering, University of Electronic Science and Technology of China, Chengdu 611731, China (e-mail: huipingduan@uestc.edu.cn).

Hongbin Li is with the Department of Electrical and Computer Engineering, Stevens Institute of Technology, Hoboken, NJ 07030 USA (e-mail: hongbin.li@stevens.edu).

Digital Object Identifier 10.1109/LSP.2020.2998357

respectively. For simplicity, we assume $\beta_m = 1, \forall m$ in the sequel of this letter.

Let $\boldsymbol{w} \in \mathbb{C}^N$ denote the beamforming vector adopted by the BS. The signal received by the user at the tth time instant is given by

$$\begin{aligned} y(t) &= \boldsymbol{h}_r^H \boldsymbol{\Theta}(t) \boldsymbol{G} \boldsymbol{w}(t) s(t) + \epsilon(t) \\ &\overset{(a)}{=} \boldsymbol{v}^H(t) \text{diag}(\boldsymbol{h}_r^H) \boldsymbol{G} \boldsymbol{w}(t) s(t) + \epsilon(t) \\ &\overset{(b)}{=} \boldsymbol{v}^H(t) \boldsymbol{H} \boldsymbol{w}(t) s(t) + \epsilon(t) \end{aligned} \tag{2}$$

where $s(t)$ is the transmitted symbol, $\epsilon(t)$ denotes the additive white Gaussian noise with zero mean and variance σ^2, in (a), we define $\boldsymbol{v} \triangleq [e^{j\theta_1} \ \ldots \ e^{j\theta_M}]^H \in \mathbb{C}^M$, and in (b), we define $\boldsymbol{H} \triangleq \text{diag}(\boldsymbol{h}_r^H)\boldsymbol{G}$. Here $\boldsymbol{H}$ is referred to as the cascade channel. An important observation based on (2) is that, in the beamforming stage, we only need the knowledge of the cascade channel $\boldsymbol{H}$ for joint active and passive beamforming, i.e., optimizing $\boldsymbol{w}$ and $\boldsymbol{v}$ to maximize the received signal power at the receiver. Therefore, in the channel estimation stage, our objective is to estimate the cascade channel $\boldsymbol{H}$ from the received measurements $\{y(t)\}_{t=1}^T$. Note that to facilitate channel estimation, different precoding vectors $\{\boldsymbol{w}(t)\}$ are employed at different time instants, while the phase shift vector $\boldsymbol{v}$ can either be time-varying or remain time-invariant over different time instants. Without loss of generality, we use $\boldsymbol{v}(t)$ to represent the phase shift vector used at the tth time instant. We also would like to clarify that the channel estimation algorithm is implemented at the receiver (i.e., user), no operation or algorithm needs to be executed at the IRS.

The cascade channel matrix $\boldsymbol{H}$ has a dimension of $M \times N$. Both N and M could be large for mmWave systems, which makes channel estimation a challenging problem. Hopefully, real-world channel measurements [12], [13] have shown that mmWave channels exhibit sparse scattering characteristics, which can be utilized to substantially reduce the training overhead.

III. Channel Model

Following [14], a narrowband geometric channel model is used to characterize the BS-IRS channel $\boldsymbol{G}$ and the IRS-user channel $\boldsymbol{h}_r$. Specifically, the BS-IRS channel can be modeled as

$$\boldsymbol{G} = \sqrt{\frac{NM}{\rho}} \sum_{l=1}^{L} \varrho_l \boldsymbol{a}_r(\vartheta_l, \gamma_l) \boldsymbol{a}_t^H(\phi_l) \tag{3}$$

where ρ denotes the average path-loss between the BS and IRS, L is the number of paths, ϱ_l denotes the complex gain associated with the lth path, ϑ_l (γ_l) denotes the azimuth (elevation) angle of arrival (AoA), ϕ_l is the angle of departure (AoD), $\boldsymbol{a}_r$ and $\boldsymbol{a}_t$ represent the receive and transmit array response vectors, respectively. Suppose the IRS is an $M_x \times M_y$ uniform planar array (UPA). We have [15]

$$\boldsymbol{a}_r(\vartheta_l, \gamma_l) = \boldsymbol{a}_x(u) \otimes \boldsymbol{a}_y(v) \tag{4}$$

where $\otimes$ stands for the Kronecker product, $u \triangleq 2\pi d \cos(\gamma_l)/\lambda$, $v \triangleq 2\pi d \sin(\gamma_l)\cos(\vartheta_l)/\lambda$, d denotes the antenna spacing, λ is the signal wavelength, and

$$\begin{aligned} \boldsymbol{a}_x(u) &\triangleq \frac{1}{\sqrt{M_x}}[1 \ e^{ju} \ \ldots \ e^{j(M_x-1)u}]^T \\ \boldsymbol{a}_y(v) &\triangleq \frac{1}{\sqrt{M_y}}[1 \ e^{jv} \ \ldots \ e^{j(M_y-1)v}]^T \end{aligned} \tag{5}$$

Due to the sparse scattering nature of mmWave channels, the number of path L is small relative to the dimensions of $\boldsymbol{G}$. Hence we can express $\boldsymbol{G}$ as

$$\boldsymbol{G} = (\boldsymbol{F}_x \otimes \boldsymbol{F}_y)\boldsymbol{\Sigma}\boldsymbol{F}_L^H \triangleq \boldsymbol{F}_P \boldsymbol{\Sigma} \boldsymbol{F}_L^H \tag{6}$$

where $\boldsymbol{F}_L \in \mathbb{C}^{N \times N_G}$ is an overcomplete matrix ($N_G \geq N$) and each of its columns has a form of $\boldsymbol{a}_t(\phi_l)$, with ϕ_l chosen from a pre-discretized grid, $\boldsymbol{F}_x \in \mathbb{C}^{M_x \times M_{G,x}}$ ($\boldsymbol{F}_y \in \mathbb{C}^{M_y \times M_{G,y}}$) is similarly defined with each of its columns having a form of $\boldsymbol{a}_x(u)$ ($\boldsymbol{a}_y(v)$), and u (v) chosen from a pre-discretized grid, $\boldsymbol{\Sigma} \in \mathbb{C}^{M_G \times N_G}$ is a sparse matrix with L non-zero entries corresponding to the channel path gains $\{\varrho_l\}$, in which $M_G = M_{G,x} \times M_{G,y}$. Here for simplicity, we assume that the true AoA and AoD parameters lie on the discretized grid. In the presence of grid mismatch, the number of nonzero entries will become larger due to the power leakage caused by the grid mismatch [16].

The IRS-user channel can be modeled as

$$\boldsymbol{h}_r = \sqrt{\frac{M}{\varepsilon}} \sum_{l=1}^{L'} \alpha_l \boldsymbol{a}_r(\vartheta_l, \gamma_l) \tag{7}$$

where ε denotes the average path-loss between the IRS and the user, α_l denotes the complex gain associated with the lth path, and ϑ_l (γ_l) denotes the azimuth (elevation) angle of departure. Due to limited scattering characteristics, the IRS-user channel can be written as

$$\boldsymbol{h}_r = \boldsymbol{F}_P \boldsymbol{\alpha} \tag{8}$$

where $\boldsymbol{\alpha} \in \mathbb{C}^{M_G}$ is a sparse vector with L' nonzero entries.

IV. Proposed Method

A. Channel Estimation

We now discuss how to develop a compressed sensing-based method to estimate the cascade channel $\boldsymbol{H}$. Let $\bullet$ denote the "transposed Khatri-Rao product," we can express the cascade channel as

$$\begin{aligned} \boldsymbol{H} &= \text{diag}(\boldsymbol{h}_r^H)\boldsymbol{G} \overset{(a)}{=} \boldsymbol{h}_r^* \bullet \boldsymbol{G} \\ &\overset{(b)}{=} (\boldsymbol{F}_P^* \boldsymbol{\alpha}^*) \bullet (\boldsymbol{F}_P \boldsymbol{\Sigma} \boldsymbol{F}_L^H) \\ &\overset{(c)}{=} (\boldsymbol{F}_P^* \bullet \boldsymbol{F}_P)(\boldsymbol{\alpha}^* \otimes (\boldsymbol{\Sigma}\boldsymbol{F}_L^H)) \\ &\overset{(d)}{=} (\boldsymbol{F}_P^* \bullet \boldsymbol{F}_P)(\boldsymbol{\alpha}^* \otimes \boldsymbol{\Sigma})(1 \otimes \boldsymbol{F}_L^H) \\ &\overset{(e)}{=} \boldsymbol{D}(\boldsymbol{\alpha}^* \otimes \boldsymbol{\Sigma})\boldsymbol{F}_L^H \end{aligned} \tag{9}$$

where in (a), $(\cdot)^*$ denotes the complex conjugate, (b) comes from (6) and (8), (c) follows from the property of Khatri-Rao product (see (1.10.27) in [17]), (d) is obtained by resorting to the property of Kronecker product (see (1.10.4) in [17]), and we define $\boldsymbol{D} \triangleq \boldsymbol{F}_P^* \bullet \boldsymbol{F}_P$ in (e). Since both $\boldsymbol{\alpha}$ and $\boldsymbol{\Sigma}$ are sparse,

their Kronecker product is also sparse. We see that after a series of transformation, a sparse representation of the cascade channel $\boldsymbol{H}$ is obtained. This sparse formulation can be further simplified by noticing that the matrix $\boldsymbol{D}$ contains a considerable amount of redundant columns due to the transposed Khatri-Rao product operation. Specifically, we have the following result regarding the redundancy of $\boldsymbol{D}$.

Proposition 1: The matrix $\boldsymbol{D} \in \mathbb{C}^{M \times M_G^2}$ only contains M_G distinct columns which are exactly the first M_G columns of $\boldsymbol{D}$, i.e.,

$$\boldsymbol{D}_u = \boldsymbol{D}(:, 1 : M_G) \tag{10}$$

where $\boldsymbol{D}_u$ denotes a matrix constructed by the M_G distinct columns of $\boldsymbol{D}$.

The proof is easily verified and thus omitted. Based on this result, the cascade channel $\boldsymbol{H}$ can be further expressed as

$$\boldsymbol{H} = \boldsymbol{D}(\boldsymbol{\alpha}^* \otimes \boldsymbol{\Sigma})\boldsymbol{F}_L^H = \boldsymbol{D}_u \boldsymbol{\Lambda} \boldsymbol{F}_L^H \tag{11}$$

where $\boldsymbol{\Lambda} \in \mathbb{C}^{M_G \times N_G}$ is a merged version of $(\boldsymbol{\alpha}^* \otimes \boldsymbol{\Sigma}) \triangleq \boldsymbol{J}$, with each of its rows being a superposition of a subset of rows in $\boldsymbol{J}$, i.e., $\boldsymbol{\Lambda}(i,:) = \sum_{n \in \mathcal{S}_i} \boldsymbol{J}(n,:)$, where $\boldsymbol{\Lambda}(i,:)$ denotes the ith row of $\boldsymbol{\Lambda}$, $\mathcal{S}_i$ denotes the set of indices associated with those columns in $\boldsymbol{D}$ that are identical to the ith column of $\boldsymbol{D}$. Clearly, there are at most $L \times L'$ nonzero entries in $\boldsymbol{\Lambda}$.

Assuming the pilot signal $s(t) = 1, \forall t$, the received signal $y(t)$ in (2) can be written as

$$\begin{aligned} y(t) &= \boldsymbol{v}^H(t)\boldsymbol{H}\boldsymbol{w}(t)s(t) + \epsilon(t) \\ &\overset{(a)}{=} \left(\boldsymbol{w}^T(t) \otimes \boldsymbol{v}^H(t)\right) \mathrm{vec}(\boldsymbol{H}) + \epsilon(t) \\ &\overset{(b)}{=} \left(\boldsymbol{w}^T(t) \otimes \boldsymbol{v}^H(t)\right) (\boldsymbol{F}_L^* \otimes \boldsymbol{D}_u)\, \mathrm{vec}(\boldsymbol{\Lambda}) + \epsilon(t) \\ &\overset{(c)}{=} \left(\boldsymbol{w}^T(t) \otimes \boldsymbol{v}^H(t)\right) \tilde{\boldsymbol{F}}\boldsymbol{x} + \epsilon(t) \end{aligned} \tag{12}$$

where (a) and (b) follow from the property of Kronecker product, and in (c) we define $\tilde{\boldsymbol{F}} \triangleq \boldsymbol{F}_L^* \otimes \boldsymbol{D}_u$ and $\boldsymbol{x} \triangleq \mathrm{vec}(\boldsymbol{\Lambda})$. Stacking the measurements collected at different time instants $\boldsymbol{y} \triangleq [y(1) \ \ \ldots \ \ y(T)]^T$, we arrive at

$$\boldsymbol{y} = \boldsymbol{\Phi}\boldsymbol{x} + \boldsymbol{\epsilon} \tag{13}$$

where $\boldsymbol{\Phi} \triangleq \boldsymbol{W}_v \tilde{\boldsymbol{F}}$ and

$$\boldsymbol{W}_v \triangleq \begin{bmatrix} \boldsymbol{w}^T(1) \otimes \boldsymbol{v}^H(1) \\ \vdots \\ \boldsymbol{w}^T(T) \otimes \boldsymbol{v}^H(T) \end{bmatrix} \tag{14}$$

So far we have converted the channel estimation problem into a sparse signal recovery problem, and many classical compressed sensing algorithms such as the orthogonal matching pursuit (OMP) [18] can be employed to estimate the sparse signal $\boldsymbol{x}$. After $\boldsymbol{x}$ is recovered, the cascade channel $\boldsymbol{H}$ can be accordingly obtained via (11).

In the following, we analyze the sample complexity of our proposed compressed sensing-based method. According to the compressed sensing theory, for an underdetermined system of linear equations $\boldsymbol{y} = \boldsymbol{A}\boldsymbol{x}$, the number of measurements required for successful recovery of $\boldsymbol{x}$ is at the order of $O(k \log n)$, where n is the dimension of $\boldsymbol{x}$, and k denotes the number of nonzero elements in $\boldsymbol{x}$. For the sparse signal recovery problem (13), we have $n = M_G N_G$ and $k \leq LL'$. Therefore our proposed method has a sample complexity of $\mathcal{O}(LL' \log(M_G N_G))$. Due to the sparse scattering nature of mmWave channels, LL' is much smaller than MN. Therefore a substantial training overhead reduction can be achieved.

B. Extension To Multi-Antenna Receiver

We briefly discuss the extension of the proposed method to the multi-antenna receiver scenario. Suppose the user is equipped with N_r antennas. Let $\boldsymbol{R} \in \mathbb{C}^{N_r \times M}$ denote the channel from the IRS to the user. Due to the sparse scattering nature of mmWave channels, we can write $\boldsymbol{R} = \boldsymbol{F}_r \boldsymbol{\Gamma} \boldsymbol{F}_P^H$ where $\boldsymbol{F}_r \in \mathbb{C}^{N_r \times N_{Gr}}$ is an overcomplete matrix and each of its columns has a form of $\boldsymbol{a}_r(\phi_i)$, with ϕ_i chosen from a pre-discretized grid, and $\boldsymbol{\Gamma} \in \mathbb{C}^{N_{Gr} \times M_G}$ is a sparse matrix with L' nonzero elements. For the MIMO scenario, the signal received by the user at the tth time instant is given by

$$y(t) = \boldsymbol{f}^H(t)\bar{\boldsymbol{H}}\boldsymbol{w}(t)s(t) + \epsilon(t) \tag{15}$$

where $\boldsymbol{f}(t)$ and $\boldsymbol{w}(t)$ denote the combining vector at the receiver and the precoding vector at the transmitter respectively, and $\bar{\boldsymbol{H}}$ is defined as

$$\begin{aligned} \bar{\boldsymbol{H}} &\triangleq \boldsymbol{R}\boldsymbol{\Theta}\boldsymbol{G} = \boldsymbol{F}_r \boldsymbol{\Gamma} \boldsymbol{F}_P^H \boldsymbol{\Theta} \boldsymbol{F}_P \boldsymbol{\Sigma} \boldsymbol{F}_L^H \\ &\triangleq \boldsymbol{F}_r \boldsymbol{\Gamma} \boldsymbol{\Xi} \boldsymbol{\Sigma} \boldsymbol{F}_L^H \end{aligned} \tag{16}$$

in which $\boldsymbol{\Xi} \triangleq \boldsymbol{F}_P^H \boldsymbol{\Theta} \boldsymbol{F}_P$. Furthermore, we have

$$\begin{aligned} \mathrm{vec}(\bar{\boldsymbol{H}}) &= \mathrm{vec}(\boldsymbol{F}_r \boldsymbol{\Gamma} \boldsymbol{\Xi} \boldsymbol{\Sigma} \boldsymbol{F}_L^H) = (\boldsymbol{F}_L^* \otimes \boldsymbol{F}_r)\mathrm{vec}(\boldsymbol{\Gamma}\boldsymbol{\Xi}\boldsymbol{\Sigma}) \\ &= (\boldsymbol{F}_L^* \otimes \boldsymbol{F}_r)(\boldsymbol{\Sigma}^T \otimes \boldsymbol{\Gamma})\mathrm{vec}(\boldsymbol{\Xi}) \\ &= (\boldsymbol{F}_L^* \otimes \boldsymbol{F}_r)(\boldsymbol{\Sigma}^T \otimes \boldsymbol{\Gamma})(\boldsymbol{F}_P^T \odot \boldsymbol{F}_P^H)\boldsymbol{v}^* \end{aligned} \tag{17}$$

where $\odot$ denotes the Khatri-Rao product. Similarly, the matrix $\bar{\boldsymbol{D}} \triangleq \boldsymbol{F}_P^T \odot \boldsymbol{F}_P^H \in \mathbb{C}^{M_G^2 \times M}$ contains only M_G distinct rows which are exactly the first M_G rows of $\bar{\boldsymbol{D}}$. Thus we can rewrite (17) as

$$\mathrm{vec}(\bar{\boldsymbol{H}}) = (\boldsymbol{F}_L^* \otimes \boldsymbol{F}_r)\bar{\boldsymbol{\Lambda}}\bar{\boldsymbol{D}}_u\boldsymbol{v}^* \tag{18}$$

where $\bar{\boldsymbol{D}}_u \triangleq \bar{\boldsymbol{D}}(1 : M_G, :)$, $\bar{\boldsymbol{\Lambda}}$ is a merged version of $\bar{\boldsymbol{J}} \triangleq \boldsymbol{\Sigma}^T \otimes \boldsymbol{\Gamma}$, i.e., $\bar{\boldsymbol{\Lambda}}(:, i) = \sum_{n \in \mathcal{Q}_i} \bar{\boldsymbol{J}}(:, n)$, where $\mathcal{Q}_i$ is the set of indices associated with those rows in $\bar{\boldsymbol{D}}$ that are identical to the ith row of $\bar{\boldsymbol{D}}$. Hence, we can move on to write

$$\begin{aligned} \mathrm{vec}(\bar{\boldsymbol{H}}) &= (\boldsymbol{F}_L^* \otimes \boldsymbol{F}_r)\bar{\boldsymbol{\Lambda}}\bar{\boldsymbol{D}}_u\boldsymbol{v}^* \\ &= \left((\bar{\boldsymbol{D}}_u\boldsymbol{v}^*)^T \otimes (\boldsymbol{F}_L^* \otimes \boldsymbol{F}_r)\right)\mathrm{vec}(\bar{\boldsymbol{\Lambda}}) \\ &\triangleq \boldsymbol{K}\bar{\boldsymbol{x}} \end{aligned} \tag{19}$$

where $\boldsymbol{K} \triangleq (\bar{\boldsymbol{D}}_u\boldsymbol{v}^*)^T \otimes (\boldsymbol{F}_L^* \otimes \boldsymbol{F}_r)$ and $\bar{\boldsymbol{x}} \triangleq \mathrm{vec}(\bar{\boldsymbol{\Lambda}})$ is a sparse vector to be estimated. Let $s(t) = 1$, and define $\boldsymbol{y} = [y(1) \ \ y(2) \ \ \ldots \ \ y(T)]^T$, we have

$$\boldsymbol{y} = \boldsymbol{W}_f\boldsymbol{K}\bar{\boldsymbol{x}} + \boldsymbol{\epsilon} \tag{20}$$

where $\boldsymbol{W}_f \in \mathbb{C}^{T \times NM}$, $\boldsymbol{W}_f(t,:) = \boldsymbol{w}^T(t) \otimes \boldsymbol{f}^H(t)$, and $\boldsymbol{W}_f(t:)$ is the tth row of $\boldsymbol{W}_f$. We see that estimation of the channel vector $\bar{\boldsymbol{x}}$ is converted to a conventional sparse signal recovery problem. Note that although we cannot obtain $\boldsymbol{\Gamma}$ (i.e., $\boldsymbol{R}$) and $\boldsymbol{\Sigma}$ (i.e., $\boldsymbol{G}$) from $\bar{\boldsymbol{x}}$, the knowledge of $\bar{\boldsymbol{x}}$ itself is enough for joint beamforming for the MIMO scenario as the joint beamforming problem can be converted to an optimization problem which maximizes $\|\bar{\boldsymbol{H}}\|_F^2 = \|\mathrm{vec}(\bar{\boldsymbol{H}})\|_2^2$ with respect to $\boldsymbol{v}$ [19], [20].

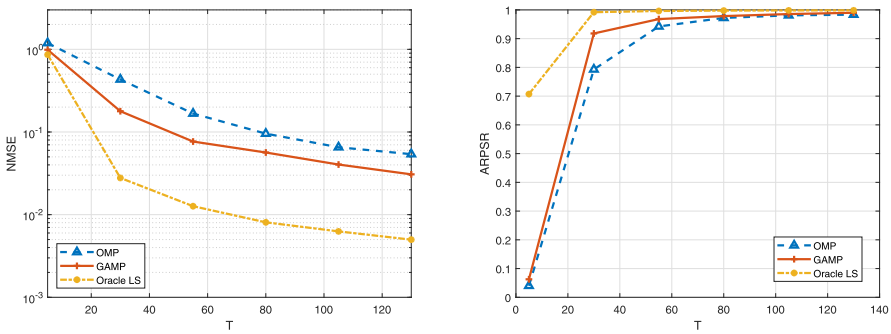

(a) NMSE. (b) ARSPR.

Fig. 1. NMSEs and ARSPRs of respective algorithms vs. T.

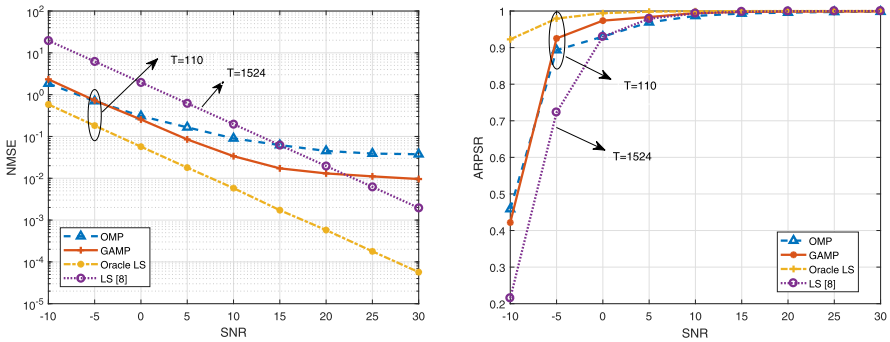

(a) NMSE. (b) ARSPR.

Fig. 2. NMSEs and ARSPRs of respective algorithms vs. SNR.

V. Simulation Results

In this section, wepresent simulation results to evaluate the performance of our proposed channel estimation method. Two different compressed sensing algorithms, namely, the OMP [18] and GAMP [21] are employed to solve (13). To provide a benchmark for our proposed method, we compare with the oracle least-squares (Oracle-LS) estimator which assumes the knowledge of the support of the sparse signal. Clearly, the oracle LS estimator provides the best achievable performance for any compressed sensing-based method. Also, we compare with the conventional LS estimator proposed in [8], which sets $T \geq NM$ and formulates channel estimation as an over-determined system of equations: $\boldsymbol{y} = \boldsymbol{W}_v \mathrm{vec}(\boldsymbol{H}) + \boldsymbol{\epsilon}$ (cf. (12)). We assume that the BS employs a uniform linear array (ULA) with $N = 16$ antennas and the IRS is a UPA consisting of $M = 8 \times 8$ passive reflecting elements. In our simulations, we set $N_G = 64$, $M_{G,x} = 32$ and $M_{G,y} = 32$. Also, we assume a Rician channel comprising a LOS path and a number of NLOS paths [22]–[24]. The Rician factor is set to 13.2 dB according to [24]. The number of paths for mmWave channels $\boldsymbol{G}$ and $\boldsymbol{h}_r$ are respectively set to $L = 3$ and $L' = 3$, where the AoA and AoD parameters are uniformly generated from $[-\pi/2, \pi/2]$ and not necessarily lie on the discretized grid.

The performance is evaluated via two metrics, i.e., normalized mean squared error (NMSE) and average receive signal power ratio (ARSPR). The NMSE is defined as $\mathbb{E}[\|(\hat{\boldsymbol{H}} - \boldsymbol{H})\|_F^2 / \|\boldsymbol{H}\|_F^2]$. The ARSPR is defined as the ratio of the actual receive signal power to the ideal receive signal power, i.e., $\mathbb{E}[\|\boldsymbol{v}^H \boldsymbol{H}\|_F^2 / \|(\boldsymbol{v}^\star)^H \boldsymbol{H}\|_F^2]$, where $\boldsymbol{v}$ and $\boldsymbol{v}^\star$ are respectively obtained via solving the joint beamforming problem [25] based on the estimated cascade channel $\hat{\boldsymbol{H}}$ and the real channel $\boldsymbol{H}$. In Fig. 1, we plot the NMSEs and ARSPRs of respective algorithms as a function of T, where the signal-to-noise ratio (SNR) is set as 10 dB. From Fig. 1, we see that GAMP only needs about 100 measurements to attain an NMSE as low as 0.04, thus achieving a substantial overhead reduction. Fig. 2 depicts the NMSEs and ARSPRs versus the SNR, where we set $T = 110$ for GAMP, OMP and the oracle LS estimator, and $T = 1524 > NM$ for the conventional LS estimator [8]. Our results show that our proposed method can achieve performance (in terms of ARPSR) close to that of the oracle LS estimator in scenarios of practical interest, e.g., $T > 40$ and SNR > -5 dB. Meanwhile, it can be observed that the conventional LS estimator [8] requires much more measurements to achieve a performance similar to the proposed method. Also, the conventional LS estimator has a computational complexity of $\mathcal{O}(T(NM)^2)$ with $T \geq NM$, while the complexity of OMP and GAMP is of $\mathcal{O}(TNM)$ with $T < NM$. Hence our proposed method is more computationally efficient than the conventional LS estimator [8].

VI. Conclusion

We studied the problem of channel estimation and joint beamforming design for IRS-assisted mmWave systems. We proposed a compressed sensing-based channel estimation method by exploiting the inherent sparse struccture of the cascade channel. Simulation results showed that our proposed method can provide an accurate channel estimation and achieve a substantial training overhead reduction.

REFERENCES

[1] C. Huang, A. Zappone, G. C. Alexandropoulos, M. Debbah, and C. Yuen, "Reconfigurable intelligent surfaces for energy efficiency in wireless communication," *IEEE Trans. Wireless Commun.*, vol. 18, no. 8, pp. 4157–4170, Aug. 2019.

[2] M. Di Renzo *et al.*, "Smart radio environments empowered by reconfigurable ai meta-surfaces: An idea whose time has come," *EURASIP J. Wireless Commun. Netw.*, vol. 2019, no. 1, pp. 1–20, 2019.

[3] Q. Wu and R. Zhang, "Intelligent reflecting surface enhanced wireless network via joint active and passive beamforming," *IEEE Trans. Wireless Commun.*, vol. 18, no. 11, pp. 5394–5409, Nov. 2019.

[4] E. Basar, M. Di Renzo, J. de Rosny, M. Debbah, M.-S. Alouini, and R. Zhang, "Wireless communications through reconfigurable intelligent surfaces," *IEEE Access*, vol. 7, pp. 116 753–116 773, 2019.

[5] X. Tan, Z. Sun, D. Koutsonikolas, and J. M. Jornet, "Enabling indoor mobile millimeter-wave networks based on smart reflect-arrays," in *Proc. IEEE Int. Conf. Comput. Commun.*, 2018, pp. 270–278.

[6] P. Wang, J. Fang, X. Yuan, Z. Chen, H. Duan, and H. Li, "Intelligent reflecting surface-assisted millimeter wave communications: Joint active and passive precoding design," 2019. [Online]. Available: https://arxiv.org/abs/1908.10734

[7] A. Taha, M. Alrabeiah, and A. Alkhateeb, "Enabling large intelligent surfaces with compressive sensing and deep learning," 2019. [Online]. Available: https://arxiv.org/abs/1904.10136

[8] D. Mishra and H. Johansson, "Channel estimation and low-complexity beamforming design for passive intelligent surface assisted MISO wireless energy transfer," in *Proc. IEEE Int. Conf. Acoust., Speech Signal Process.*, 2019, pp. 4659–4663.

[9] T. L. Jensen and E. D. Carvalho, "On optimal channel estimation scheme for intelligent reflecting surfaces based on a minimum variance unbiased estimator," in *Proc. IEEE Int. Conf. Acoust., Speech Signal Process. (ICASSP)*, Barcelona, Spain, May 4–8, 2020, pp. 5000–5004.

[10] Z. He and X. Yuan, "Cascaded channel estimation for large intelligent metasurface assisted massive MIMO," *IEEE Wireless Commun. Lett.*, vol. 9, no. 2, pp. 210–214, Feb. 2020.

[11] B. Zheng and R. Zhang, "Intelligent reflecting surface-enhanced OFDM: Channel estimation and reflection optimization," *IEEE Wireless Commun. Lett.*, vol. 9, no. 4, pp. 518–522, Apr. 2020.

[12] T. S. Rappaport *et al.*, "Millimeter wave mobile communications for 5G cellular: It will work!" *IEEE Access*, vol. 1, pp. 335–349, May 2013.

[13] M. R. Akdeniz *et al.*, "Millimeter wave channel modeling and cellular capacity evaluation," *IEEE J. Sel. Areas Commun.*, vol. 32, no. 6, pp. 1164–1179, Jun. 2014.

[14] A. Alkhateeb, O. E. Ayach, G. Leus, and R. Heath, "Channel estimation and hybrid precoding for millimeter wave cellular systems," *IEEE J. Sel. Topics Signal Process.*, vol. 8, no. 5, pp. 831–846, Oct. 2014.

[15] Y. Ding and B. D. Rao, "Dictionary learning-based sparse channel representation and estimation for FDD massive MIMO systems," *IEEE Trans. Wireless Commun.*, vol. 17, no. 8, pp. 5437–5451, Aug. 2018.

[16] Y. Chi, L. L. Scharf, A. Pezeshki, and A. R. Calderbank, "Sensitivity to basis mismatch in compressed sensing," *IEEE Trans. Signal Process.*, vol. 59, no. 5, pp. 2182–2195, May 2011.

[17] X.-D. Zhang, *Matrix Analysis and Applications*, Cambridge, U.K.: Cambridge Univ. Press, 2017.

[18] J. A. Tropp and A. C. Gilbert, "Signal recovery from random measurements via orthogonal matching pursuit," *IEEE Trans. Inf. Theory*, vol. 53, no. 12, pp. 4655–4666, Dec. 2007.

[19] B. Ning, Z. Chen, W. Chen, and J. Fang, "Beamforming optimization for intelligent reflecting surface assisted MIMO: A sum-path-gain maximization approach," *IEEE Wireless Commun. Lett.*, to be published, doi: 10.1109/LWC.2020.2982140.

[20] S. Zhang and R. Zhang, "Capacity characterization for intelligent reflecting surface aided MIMO communication," 2019. [Online]. Available: https://arxiv.org/abs/1910.01573

[21] J. P. Vila and P. Schniter, "Expectation-maximization Gaussian-mixture approximate message passing," *IEEE Trans. Wireless Commun.*, vol. 61, no. 19, pp. 4658–4672, Oct. 2013.

[22] S. Hur, T. Kim, D. J. Love, J. V. Krogmeier, T. A. Thomas, and A. Ghosh, "Millimeter wave beamforming for wireless backhaul and access in small cell networks," *IEEE Trans. Commun.*, vol. 61, no. 10, pp. 4391–4403, Oct. 2013.

[23] X. Li, J. Fang, H. Duan, Z. Chen, and H. Li, "Fast beam alignment for millimeter wave communications: A sparse encoding and phaseless decoding approach," *IEEE Trans. Signal Process.*, vol. 67, no. 17, pp. 4402–4417, Sep. 2019.

[24] Z. Muhi-Eldeen, L. Ivrissimtzis, and M. Al-Nuaimi, "Modelling and measurements of millimetre wavelength propagation in urban environments," *Microw., Antennas Propag.*, vol. 4, no. 9, pp. 1300–1309, 2010.

[25] X. Yu, D. Xu, and R. Schober, "MISO wireless communication systems via intelligent reflecting surfaces," in *Proc. IEEE/CIC Int. Conf. Commun. China*, 2019, pp. 735–740.